Supplementary Information

Concurrent production of a diesel valeric biofuel and a fuel additive in a one-pot process over SiO_2-Al_2O_3-supported catalysts: Influence of the Si/Al ratio

Francisco A. Martínez, Darío J. Segobia, Nicolás M. Bertero*

Catalysis Science and Engineering Research Group (GICIC),

INCAPE, UNL-CONICET, CCT Conicet- Paraje El Pozo,

(3000), Santa Fe, Argentina.

SI.1. Material selection, sample conditioning and catalyst characterization

Commercial SiO_2-Al_2O_3 (SA) samples with different Si/Al ratios were selected for this study (SIRAL-10, SIRAL-40, SIRAL-70 from SASOL and Grade 135 from Sigma-Aldrich), named from now on SA-0.09, SA-0.57, SA-1.98 and SA-6.06, respectively, according to their Si/Al molar ratio. Before characterization and catalytic tests all these samples were calcined in air flow at 500 °C (60 cm^3/min) for 2 h.

The bifunctional catalyst Rh/SA-6.06 employed in this work was prepared by incipient wetness impregnation of SA-6.06 sample at room temperature using an aqueous solution of $RhCl_3$ (Aldrich 98%). The impregnated sample was dried for 12 h at 100 °C, then heated in air at 5 °C/min to 450 °C for 3 h. Prior to characterization and catalytic tests, this calcined sample was activated in H_2 flow (60 cm^3/min) for 2 h at 450 °C.

Elemental composition of the commercial SA samples and the impregnated Rh/SA-6.06 sample was determined by energy dispersive X-ray fluorescence spectrometry (EDXRF) using a Shimadzu EDX-720 spectrometer.

Textural properties such as BET surface area (S_g), pore volume (V_P) and pore size distribution were determined by N_2 physisorption at -196 °C in a Quantochrome Corporation NOVA-1000 sorptometer.

Particle size distribution of SiO_2-Al_2O_3 samples was determined by dynamic image analysis, using a Camsizer XT particle analyzer from Retsch Technology. In all the cases, the X-Jet dispersion module was set at 10 kPa air dispersion pressure.

The Lewis/Brønsted nature of surface acid sites on SA samples was determined by Fourier transform infrared spectroscopy (FTIR) using pyridine as probe molecule and a Shimadzu FT-IR-8101M spectrophotometer [1]. Surface acid density and relative acid strength were determined by temperature-programmed desorption (TPD) of NH_3 pre-adsorbed at 100 °C on reduced samples as described elsewhere [1].

The relative reducibility of metal oxides in the calcined Rh/SA-6.06 sample was determined by temperature-programmed reduction (TPR). The TPR profile was obtained passing a H_2(5%)/Ar gaseous mixture at 60 cm^3 (STP) min^{-1} through a 150 mg-fixed bed of the sample, while heating from room temperature to 800 °C at 10 °C/min. H_2 consumption was quantified by mass spectrometry (MS) in a Baltzers Omnistar unit [1].

The calcined Rh/SA-6.06 sample was analysed by X-ray diffraction (XRD) using a PANalytical Empyrean diffractometer and Ni-filtered Cu-Kα radiation (40 kV y 45 mA) and scanning at a speed of 2 º min^{-1}.

Transmission electron microscopy (TEM) was performed using a JEOL 2100 plus microscope. Previously, the Rh/SA-6.06 sample was reduced ex situ under H_2 (100 %) flow at the temperatures described previously for 2 h, cooled down to room temperature in N_2 flow

and then passivated in an O_2(2%)/N_2 stream. Then, the reduced/passivated sample powder was dispersed in milli-Q water. After 30 s in an ultrasonic bath, a drop of this suspension was applied to a copper grid (200 mesh) coated with carbon film, and it was allowed to dry in air. More than 130 particles randomly taken from at least five TEM images were measure to estimate the average metal particle size by the expression $\bar{d}_M = \frac{\sum_{i=1}^{n} n_i \cdot d_i^3}{\sum_{i=1}^{n} n_i \cdot d_i^2}$, where n_i is the number of particles having a d_i diameter.

The amount of carbon (coke) deposited on catalysts during catalytic activity tests was measured by temperature-programmed oxidation (TPO). Catalytic samples were collected from the reactor by filtration and then dried at 100 °C overnight. Then 15-20 mg of dried sample was treated in N_2 flow for 1 h at 90 °C to eliminate weakly adsorbed molecules of GVL, PeOH or products. Then, samples were heated in a O_2(2%)/N_2 stream at 10 °C.min^{-1} from room temperature to 800 °C. The evolved CO_2 was converted into methane in a fixed bed methanation reactor containing a Ni-based catalyst (Ni/kieselguhr) at 400 °C and monitored in an SRI 8610C gas chromatograph equipped with a flame ionization detector (FID).

SI.2. Catalytic tests

Catalytic tests were performed in liquid phase in a commercial stirred tank reactor (Parr 4565) with a capacity of 100 mL, equipped with mechanic stirrer and operated in batch mode. The particular dimensions of the reactor can be found in the webpage of the company [2]. In the catalytic activity experiments 1.5 mL GVL (99%, Sigma-Aldrich), 40 mL of PeOH (pentanol 99%, Sigma-Aldrich), 0.5 mL of hexadecane (99%, Sigma-Aldrich) used as internal standard and 0.25 g of catalyst (activated ex-situ) were charged in inert N_2 atmosphere to the reactor. In these conditions, PeOH played both roles as reactant and solvent and the initial concentration of GVL was 0.37 M. Then, the reactor was heated up to 250 °C and the pressure was rapidly increased up to the reaction value with N_2 or H_2, depending on the case. The bare SA samples were tested using 10 bar of N_2, whereas the Rh/SA-6.06 sample was tested employing 15 bar of H_2. This sudden increase of the pressure pushes GVL, initially inside a stainless-steel tube, into the reactor. Thus, any conversion of the GVL during heating stage was avoided. The zero time of reaction was considered when the pressure inside the reactor reached the autogenous pressure plus 10 (with N_2) or 15 bar (with H_2), and

the reaction was carried out during 8 h from that initial time. Stirring speeds of 650 rpm and particle sizes lower than 150 μm were used to minimize mass transfer limitations [1].

Liquid samples were carefully withdrawn from the reactor every 5-30 min by using a loop under pressure. This loop avoided flushing of volatile components when the sample was depressurized. Previously to withdraw a liquid sample, the loop was flushed twice with N_2 and then pressurized with this gas to 4 bar. After withdrawing a sample, this loop was flushed again with N_2 in order to avoid contamination of the following sample. Using this sampling methodology, the repeatability of experiments was verified, observing a narrow dispersion (about 2%) among the compositions of the liquid samples. The total volume of all withdrawn samples (including eventual waste for flushing the loop) in all the cases was about 5 mL, i.e. less than 15% of the volume of the initial reaction mixture. Concentrations of unreacted GVL and reaction products were determined by ex situ gas chromatography.

Concentrations of unreacted GVL and reaction products were followed by ex situ gas chromatography using an Agilent 6850 chromatograph equipped with flame ionization detector (heated at 300 °C), temperature programmer, and a HP-1 capillary column (50 m × 0.32 mm ID, 1.05 μm film).

The reactant conversion (X_{GVL}, mol of GVL reacted/mol of GVL fed) was calculated as $X_{GVL}(\%) = \frac{C_{GVL}^{0} - C_{GVL}}{C_{GVL}^{0}} \cdot 100$, where C^0_{GVL} is the initial GVL concentration and C_{GVL} is the GVL concentration at reaction time *t*. Yields (η_j, mol of product j/mol of GVL fed) were calculated as $\eta_j(\%) = \frac{C_j}{C_{GVL}^{0}} \cdot 100$, where C_j is the concentration of product j. Selectivities (S_j, mol of product j/mol of GVL reacted) were calculated as $S_j(\%) = \frac{C_j}{C_{GVL}^{0} - C_{GVL}} \cdot 100$. Carbon balance was estimated as $CB(\%) = \frac{C_{GVL} + \sum C_j}{C_{GVL}^{0}} \cdot 100$, where $\sum C_j$ is the total product concentration.

Catalyst stability tests were carried out with a Rh(1%)/SA-6.06 bifunctional sample and comprised three consecutive catalytic runs of 8 h. When a run was finished, the reactor was cooled down and the catalyst was separated by filtration, dried for 12 h at 100 °C, calcined in air flow at 500 °C (60 $cm^3\ min^{-1}$) for 2 h and finally activated in H_2 flow (60 $cm^3\ min^{-1}$) for 2 h at 450 °C. The activated sample was loaded into the reactor in N_2 atmosphere for the following run.

SI.3. Additional results from the characterization of SA samples

The summary of the characterization results for the SA samples was presented in Table 1 of the manuscript. The Si/Al ratio of these samples, determined by EDXRF, was between 0.09 and 6.06.

The N_2 adsorption/desorption isotherms at -196 °C for SA samples are shown in Figure SI.1. All the samples exhibited the hysteresis cycle characteristic of Type IV isotherms (IUPAC classification), which indicates the presence of mesopores. From these results it was possible to estimate the main textural properties (S_g and V_P) that are shown in Table 1 of the manuscript. Regarding the average pore diameter of SA samples, the values of 44, 49, 114 and 50 Å were determined for SA-0.09, SA-0.57, SA-1.98 and SA-6.06, respectively.

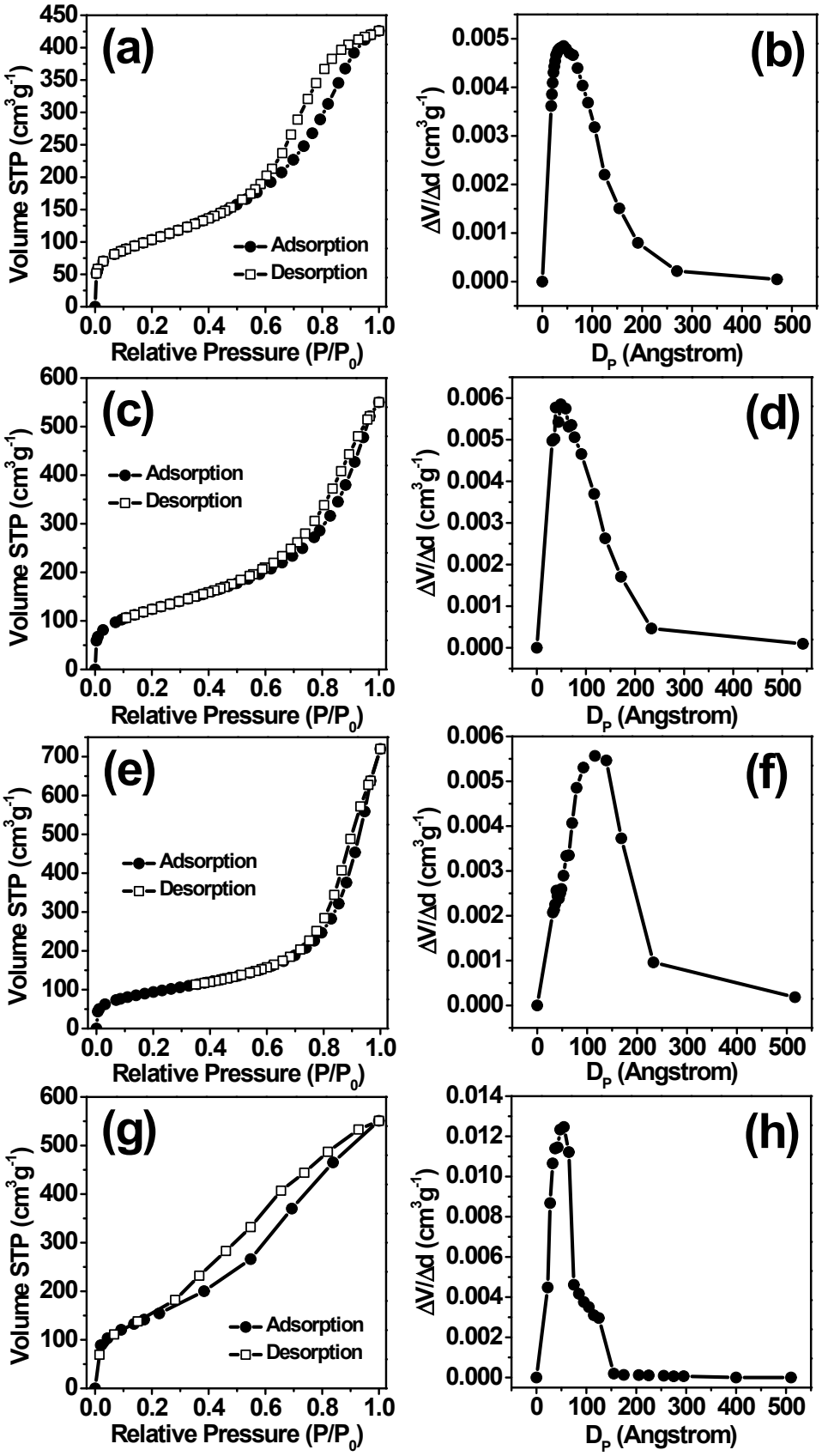

Figure SI.1: N_2 adsorption/desorption isotherms at -196 °C of (a) SA-0.09, (c) SA-0.57, (e) SA-1.98 and (g) SA-6.06 and pore size distribution of (b) SA-0.09, (d) SA-0.57, (f) SA-1.98 and (h) SA-6.06.

The results of particle size distribution analysis are shown in Figure SI.2. From the relative distribution curve (Figure SI.2.a), the average particle size for SA-0.09, SA-0.57 and SA-1.98 was approximately 45 μm, whereas for the sample SA-6.06 it was 62 μm. From the cumulative distribution curve (Figure SI.2.b), it is possible to see that 50% of the particles are smaller than 44 μm for SA-0.09, SA-0.57 and SA-1.98, whereas in the case of SA-6.06 50% of the particles are smaller than 63 μm. This can be due to differences in the synthesis method carried out by the two different manufacturers (SASOL and Merck). However, analyzing the Q3 curve (Figure SI.2.b), it is possible to infer that practically all the particles in the four SA samples are smaller than 150 μm. This result is very useful for the evaluation of mass transfer limitations carried out in Section SI.6.

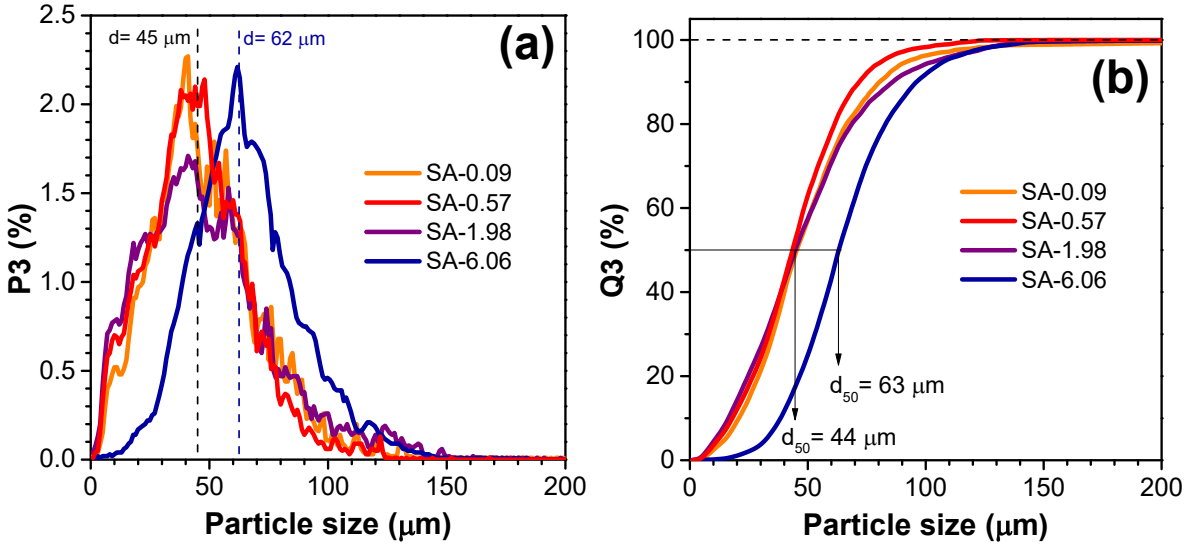

Figure SI.2: particle size distribution of SiO_2-Al_2O_3 samples determined by dynamic image analysis: (a) relative distribution (P3) and (b) cumulative distribution (Q3) of particle size.

SI.4. Additional catalytic results in the conversion of GVL in the presence of PeOH over SA samples

Initially, a “blank” test without catalyst contacting only GVL and PeOH at 250 °C and 10 bar of N_2 was performed. In this experiment, no conversion of GVL was observed after 8 h. Then, GVL was put in contact with PeOH for 8 h in the presence of the SA samples selected for this study, at 10 bar of N_2 and 250 °C and the results (except for SA-1.98 sample shown in the manuscript) are shown in Figure SI.3.

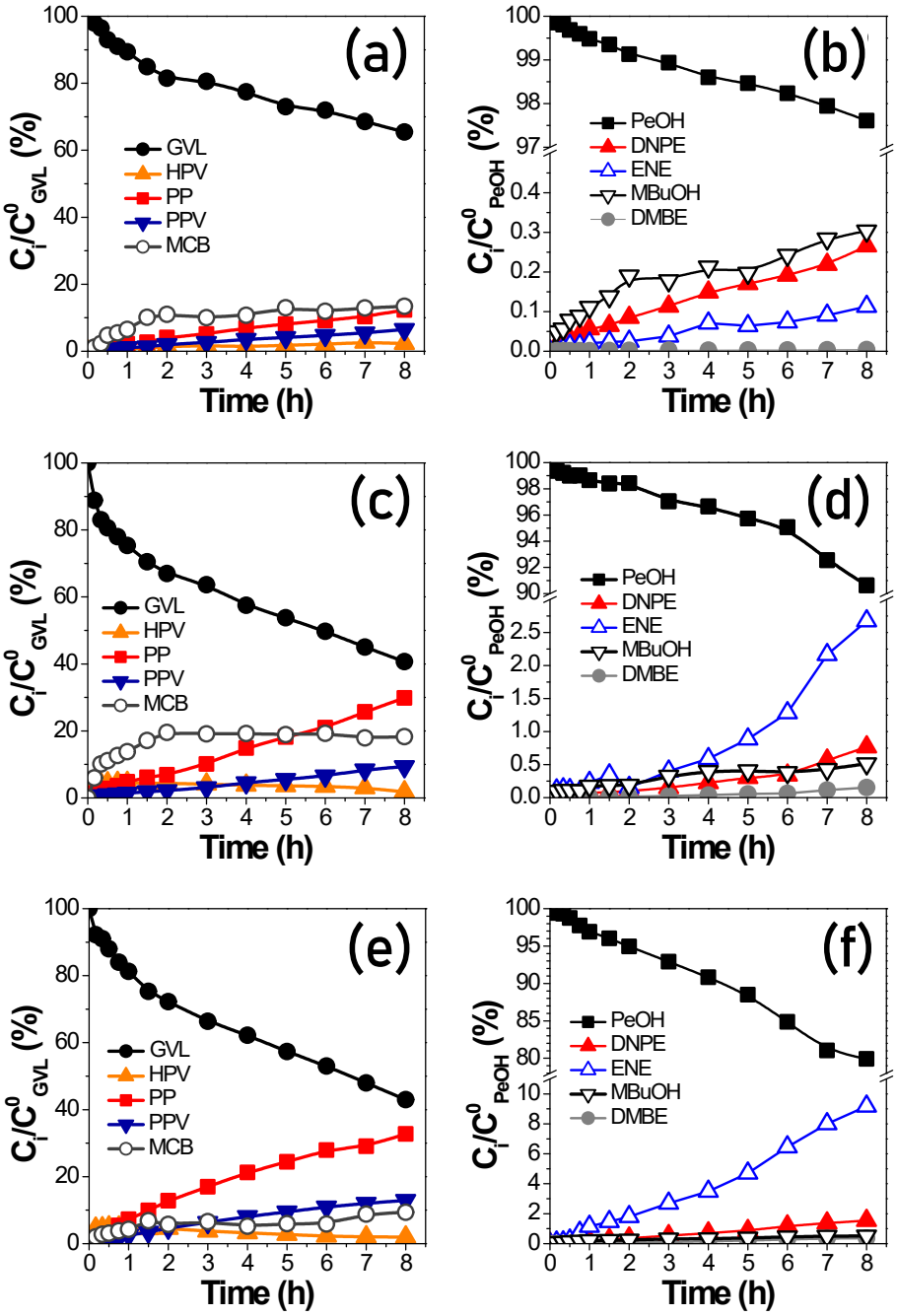

Figure SI.3: Conversion of GVL and PeOH over SA-0.09 (a-b); SA-0.57 (c-d) and SA-6.06 (e-f) [T=250 °C, p=10 bar (N_2), W_C=0.25 g, V_{PeOH}=40 mL, C^0_{GVL}= 0.37 M, stirring rate= 650 rpm, time= 8 h].

The evolutions with time of the products were similar for all the samples and were in total agreement with the reaction scheme of Figure 1 of the manuscript, also reported by other authors [3]. In the first step, the ring-opening of GVL took place by the action of the PeOH, forming HPV as primary product. This intermediate product led to the desired PP intermediate by intramolecular dehydration and to the undesired PPV by intermolecular dehydration with PeOH. For all the tested SA samples the production of PP was higher than

that of PPV, and as it was mentioned in the manuscript, no production of PV from PP was observed over the SA samples, due to the lack of H_2 and a metal catalytic function. Over the SA samples the GVL conversion was between 35.0 and 66.2% (Table 2), though as it is explained in the manuscript, the conversion of GVL over SiO_2-Al_2O_3-supported bifunctional catalysts is usually higher due to the shifting of the equilibrium of the acid-catalysed reactions by consumption of PP by hydrogenation to PV over the metal sites.

SI.5. Characterization results of the Rh/SA-6.06 bifunctional catalyst

The metal loading for Rh/A-6.06 catalyst, determined by EDXRF, was 0.94 %wt. The final chlorine content in the activated sample was 0.61 wt%, due to an incomplete elimination of Cl from the metal precursor during the calcination and activation processes.

The N_2 adsorption/desorption isotherms at -196 °C for the Rh/SA-6.06 sample are shown in Figure SI.4.a. This bifunctional catalyst also showed the hysteresis cycle characteristic of Type IV isotherms (IUPAC classification) confirming the presence of mesopores. The main textural properties of this catalyst were a specific surface area of S_g=392 m^2/g and a total pore volume of V_P=0.57 cm^3/g. Both values, S_g and V_P indicated that a partial blockage of the pore structure of the SA-6.06 support took place after the impregnation process with $RhCl_3$.The pore size distribution of Rh/SA-6.06, shown in Figure SI.4.b, revealed that the average pore diameter is 47 Å in this sample.

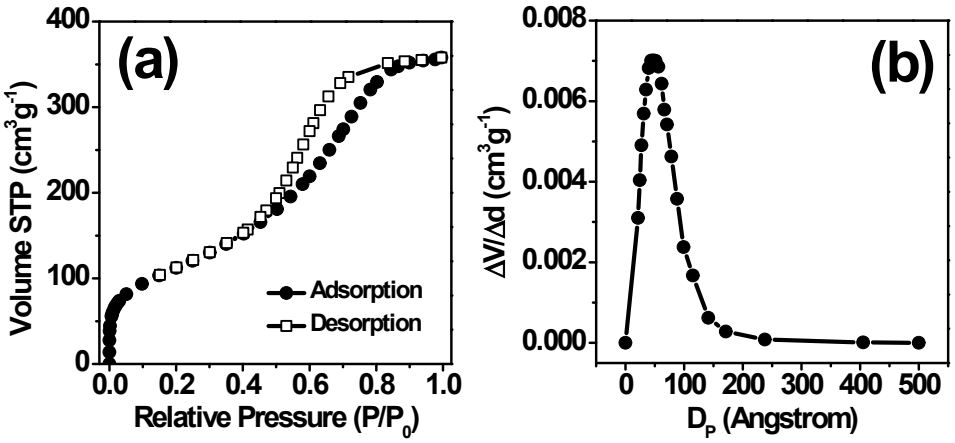

Figure SI.4: (a) N_2 adsorption/desorption isotherms at -196 °C and (b) pore size distribution for the Rh/SA-6.06 bifunctional catalyst.

It is worth mentioning that the particle size distribution of Rh/SA-6.06 catalyst was identical to that obtained for the bare support SA-6.06 (shown in Figure SI.2).

The X-Ray diffractogram of the calcined Rh/SA-6.06 sample, shown in Figure SI.5, only exhibited the characteristic amorphous halo of the SA support between 15 and 35°. This

strongly suggested a high dispersion of the metal oxides particles over the SA-6.06 support, probably with crystalline domains of the oxides smaller than 4 nm.

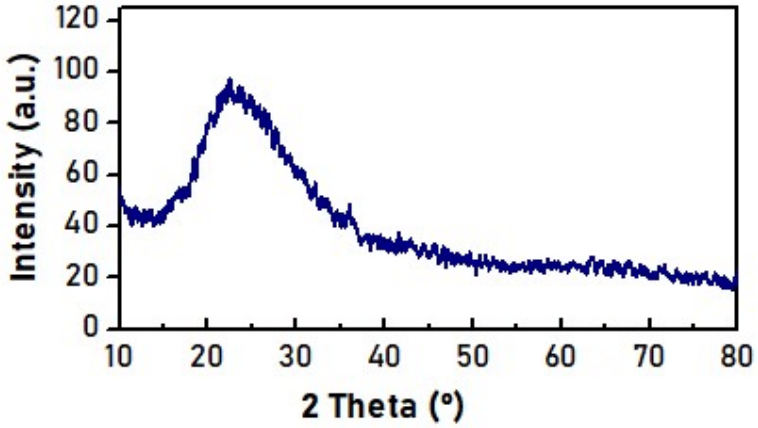

Figure SI.5: XRD pattern of the activated Rh/SA-6.06 bifunctional catalyst.

The temperature-programmed reduction profile of the calcined Rh/SA-6.06 sample is shown in Figure SI.6. This profile showed a single reduction peak between 100 °C and 180 °C, showing its maximum at about 134 °C, in agreement with the reduction of Rh oxide particles observed by other authors [4].

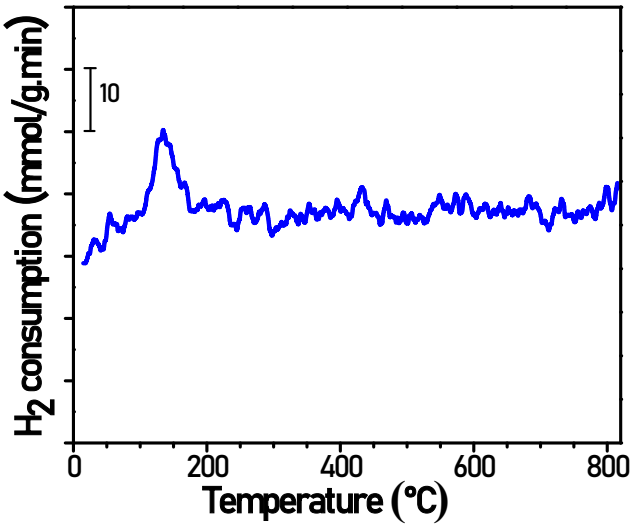

Figure SI.6: Temperature-programmed reduction of the calcined Rh/SA-6.06 sample [heating rate: 10 °C/min; 60 cm^3/min of H_2(5%)/Ar].

The size of the metal particles in the activated Rh/SA-6.06 sample was determined by transmission electron microscopy (TEM). From the analysis of TEM images, shown in Figure SI.7.a-e, it is possible to infer that Rh/SA-6.06 sample exhibited a relatively wide metal particle size distribution, containing particles from 1-2 nm up to 10 nm (Figure SI.7.f).

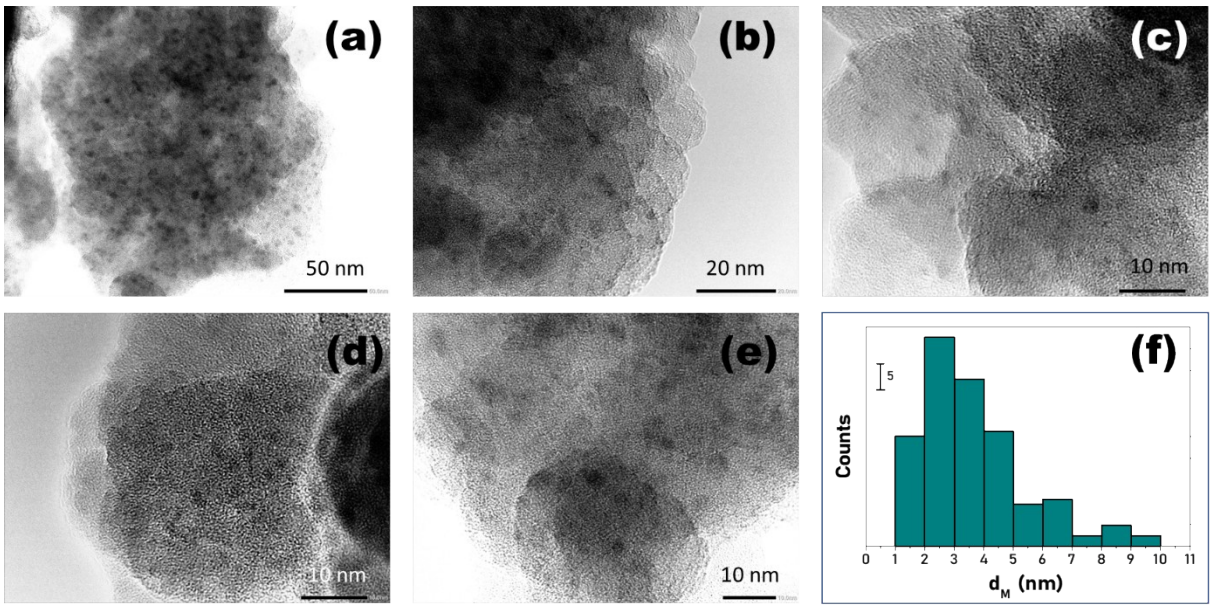

Figure SI.7: (a)-(e) TEM images and (f) metal particle size distribution of the activated Rh/SA-6.06 bifunctional catalyst determined from the TEM images.

This relative wide range of sizes make the estimation of the average metal particle size by the arithmetic mean not suitable for characterizing catalytic materials, and for this reason the volume-area average, determined by

$$\bar{d}_M = \frac{\sum_{i=1}^{n} n_i \cdot d_i^3}{\sum_{i=1}^{n} n_i \cdot d_i^2}$$

was employed [5]. Thus, an average value of 5.6 nm was estimated.

Regarding acid properties, the acid density and relative acid strength of reduced Rh/SA-6.06 catalyst were probed by TPD of NH_3 preadsorbed at 100 °C, the same as with the SA samples, and the results are shown in Figure SI.8. Similarly, the total acid site density was considered as the contribution of three bands with different strength: (a) relatively weak acid sites that desorb NH_3 with the maximum rate at temperatures in the range 150-250 °C; (b) acid sites of intermediate strength which show the maximum desorption rate between 250 and 450 °C and (c) strong acid sites that desorb the NH_3 exhibiting the maximum rate over 500 °C. For Rh/SA-6.06 catalyst, the maximum desorption rate of these three bands were at 247 °C, 349 °C and 547 °C, i.e. only the weaker acid sites in Rh/SA-6.06 are stronger than in the bare support SA-6.06. The total acid site for the Rh/SA-6.06 sample was 211.7 μmol/g. Regarding the proportion of these acid sites to the total acid site density, the relatively weak sites represented the 20.4% of the total acid site, acid sites with an intermediate strength the 42.4% and the strongest acid sites were the 37.1% of the total acid site. This suggested that

the deposition of the chlorinated noble metal precursor modified, in a certain degree, the acidity of the support, as we suggested in a previous work [5].

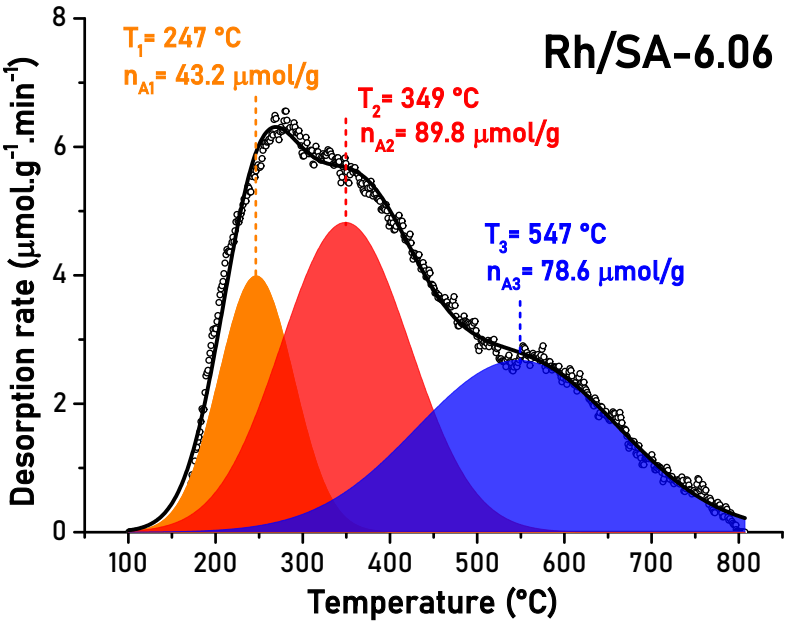

Figure SI.8: Temperature-programmed desorption of NH_3 over the Rh/SA-6.06 sample [heating rate: 10 °C/min; He flow=60 cm^3/min; W_C= 150 mg].

The nature of surface acid sites on the activated Rh/SA-6.06 sample was determined by FTIR of pyridine chemisorbed on the sample. The FTIR spectrum for this bifunctional catalyst, obtained in the wavenumber range 1400-1700 cm^{-1}, is shown in Figure SI.9.

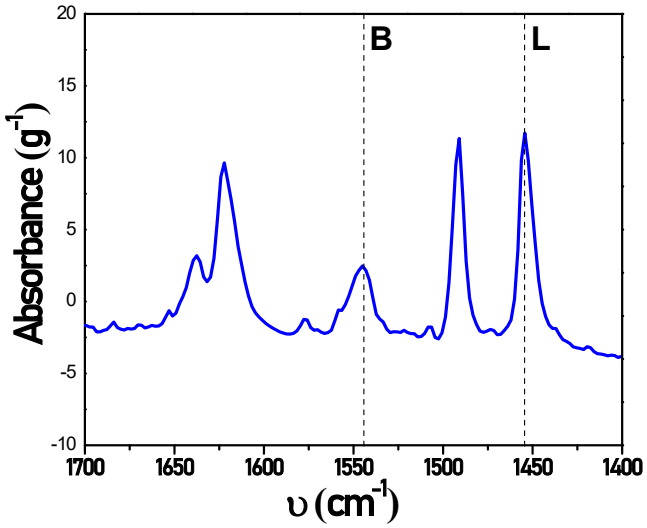

Figure SI.9: FTIR spectrum after pyridine adsorption at room temperature and evacuation at 150 °C on the activated Rh/SA-6.06 bifunctional catalyst [L: Lewis; B: Brønsted sites].

The IR bands at around 1540 cm^{-1} and 1440-1460 cm^{-1} correspond to pyridine chemisorbed on Brønsted (B) and Lewis (L) sites, respectively [6]. The integration of these bands made possible to estimate the proportion of Lewis acid sites to total acid sites showing L/(L+B)=0.65, indicating that not only the total density and strength of acid sites changed with the impregnation process, but also their Lewis/Brønsted nature. In this case, proportion of Lewis acid sites diminished considerably from 0.79 in the bare SA-6.06 support up to 0.65 in the Rh/SA-6.06 catalyst. This strongly suggests that the presence of chlorine on the surface modified the Lewis/Brønsted balance of the acid sites. The creation of new HO- groups with a Brønsted character on the surface of SA and γ-Al_2O_3 by the adsorption of HCl is a well-known phenomenon [7]. This modification of the surface acidity takes place by the formation of a hydroxyl ion from HCl and an oxide ion that attaches a chloride ion at an adjoining vacant site and could take place with several noble metal-based catalysts [5].

SI.6. Evaluation of mass transfer limitations with Rh/SA-6.06 bifunctional catalyst

The absence of liquid-solid and intraparticle mass transfer limitations was verified employing the Ramachandran-Chaudhari [8] and Weisz-Prater [9] criteria. The analysis was carried out for the γ-valerolactone and pentanol, considering that both species are the only involved in the first acid catalyzed reaction of the one-pot process.

SI.6.1. Mass transfer limitations in the liquid/solid interphase

According to the Ramachandran-Chaudhari criterion [8], no significant mass transfer limitations exist for reactant *i* if dimensionless index $\alpha_{2,i} < 0.1$:

$$\alpha_{2,i} = \frac{\left(r_i^V\right)_{obs}}{k_s \cdot a_p \cdot w_C \cdot C_i} \qquad \text{(Eq. SI-1)}$$

where:

$\left(r_i^V\right)_{obs}$: experimental volumetric conversion rate of reactant *i* (mol s^{-1} cm^{-3}).

C_i: concentration of reactant *i* in liquid phase (mol cm^{-3}).

$k_{s\,i}$: mass transfer coefficient for reactant *i* (cm s^{-1}).

a_p: specific external surface area of catalyst particles (cm^2 g^{-1}).

w_C: catalyst concentration (g cm^{-3}).

To calculate α_2, the initial values of r_i^V and C_i were employed, i.e. r_{GVL}^0 and C_{GVL}^0 in the case of γ-valerolactone (GVL) and r_{PeOH}^0 and C_{PeOH}^0 for pentanol (PeOH) It is worth

mentioning that r_{GVL}^{0} and r_{PeOH}^{0} values were those obtained over Rh/SA-6.06, because the initial reaction rate for GVL and PeOH showed the highest values, i.e. the worst-case scenario for mass transfer limitations. The mass transfer coefficient for GVL ($k_{s,GVL}$) and PeOH ($k_{s,PeOH}$) was determined using the correlation of Sano et al. [10].

$$Sh_P = \left[2 + 0.4 \cdot \left(\frac{\varepsilon . d_p^4}{V^3}\right)^{1/4} \cdot Sc^{1/3}\right] \cdot F_C \qquad \text{(Eq. SI-2)}$$

where:

Sh_P: Sherwood number (dimensionless)

ε: energy supplied to the liquid by the impeller

d_P: particle diameter (cm)

ν: kinematic viscosity (cm^2 g^{-1})

Sc: Schmidt number (dimensionless).

F_C: shape factor, assumed equal to 1 for spherical particles (dimensionless).

$$Sh_P = \frac{k_s . d_p}{D_{i\,m}} \qquad \text{(Eq. SI-3)}$$

$$Sc = \frac{\mu_L}{\rho_L . D_{i\,j}} \qquad \text{(Eq. SI-4)}$$

$$\varepsilon = \frac{N_P \cdot {d_I}^5 \cdot n^3}{V} \qquad \text{(Eq. SI-5)}$$

$$a_p = \frac{6}{d_P \cdot \rho_P} \qquad \text{(Eq. SI-6)}$$

with:

D_{ij}: diffusivity of reactant *i* in the liquid phase (cm^2 min^{-1})

μ_L: liquid viscosity (g cm^{-1} s^{-1})

ρ_L: density of the liquid phase (g cm^{-3})

N_P: power number (dimensionless)

d_I: impeller diameter (cm)

n: impeller speed (rpm)

V: volume of the liquid (cm^3)

ρ_P: density of the particle (g cm^{-3})

D_{ij}, or the diffusion coefficient for *i* in the binary GVL-PeOH mixture, was estimated with the equation of Vignes [11] using the estimates of the diffusion coefficients in the dilute solution limit $D°_{ij}$ and $D°_{ji}$ and the molar compositions (x_i and x_j) in the initial reaction mixture.

$$D_{ij} = \left(D°_{ij}\right)^{x_j} \cdot \left(D°_{ji}\right)^{x_i} \quad \text{(Eq. SI-7)}$$

$D°_{ij}$ was estimated with the correlation of Wilke and Chang [12], the most widely used correlation for estimation of the diffusion coefficients in the dilute solution limit. In general, the association coefficient is unity for non-associating components, between one and two for associating components and larger than two for highly associating components and water. In the case of GVL and PeOH, α_{GVL}=2.58 and α_{PeOH}=2.55, respectively [13],[14].

$$D°_{is} = \frac{7.4x10^{-8} \cdot T \cdot \sqrt{\alpha_s \cdot MW_s}}{\eta_s \cdot \left(\alpha_i \cdot V_i\right)^{0.6}} \quad \text{(Eq. SI-8)}$$

where:

$D°_{is}$: diffusivity of component *i* in the solvent in the dilute solution limit ($cm^2\ s^{-1}$).

T: absolute temperature (K).

α_S: association coefficient of the solvent.

α_i: association coefficient of the component *i*.

MW_S: molecular weight of the solvent ($g\ mol^{-1}$)

V_i: volume of the component *i* at its normal boiling point ($cm^3\ mol^{-1}$).

η_s: solvent viscosity (cP).

The viscosity of the pure components GVL and PeOH at the reaction temperature (250 °C) was estimated employing a well-known correlation [15].

Using a conservative estimation of the Sherwood number ($Sh_P = 2$) a minimum value of the mass transfer coefficient can be determined, giving the worst-case scenario for significant mass transfer limitations. It is worth mentioning that the value of the mass transfer coefficient can be one or two order of magnitude higher than these underestimated values. Table S1 shows the $k_{s,i}$ and α_{2i} values obtained using the initial GVL and PeOH conversion rates experimentally determined.

Table S1: Values of volumetric initial conversion rate (r_i^0), mass transfer coefficient ($k_{s,i}$) and parameter $\alpha_{2,i}$ determined for GVL and PeOH.

Reactant *i*	r_i^{v0} (mol s^{-1} cm^{-3})	$k_{s,i}$ (cm s^{-1})	$\alpha_{2,i}$
GVL	2.84 x10^{-8}	2.91 x10^{-2}	4.38 x10^{-4}
PeOH	5.98 x10^{-8}	2.44 x10^{-1}	4.68 x10^{-6}

In both cases, for GVL and PeOH, the α_2 value was significantly lower than 10^{-1}, thereby indicating the absence of significant liquid-solid mass transfer limitations.

SI.6.2. Intraparticle mass transfer limitations

The significance of intraparticle mass transfer limitations was determined by using the criteria of Weisz-Prater [9]. The Weisz-Prater criterion considers that pore diffusion limitations are negligible if parameter Φ (Eq. SI-9) is much lower than 1.

$$\Phi_i = \frac{(r_i^V)_{OBS}.L^2}{D_i^e.C_i} \qquad \text{(Eq. SI-9)}$$

where:

L: characteristic length of the solid particle (cm).

D_i^e: effective diffusivity of reactant *i* inside the porous channels (m^2 s^{-1}).

$(r_i)_{obs}$: experimental extensive conversion rate of reactant *i* (mol min^{-1}).

The effective diffusivity of reactant *i* inside the catalyst particles was calculated with:

$$D_i^e = \frac{\varepsilon \cdot D_{ij}}{\tau} \qquad \text{(Eq. SI-10)}$$

where:

ε: porosity of the catalyst (dimensionless).

τ: tortuosity factor of the catalyst (dimensionless).

Values of ε = 0.5 and τ = 3.0 [16] were used in the estimation of effective diffusivity.

Parameter L was calculated as:

$$L = \frac{d_P}{6} \qquad \text{(Eq. SI-11)}$$

Table S2 shows values of volumetric and extensive initial conversion rates (r_i^{0V} and r_i^0, respectively), diffusivities of reactant *i* (D_{ij} and D_{ij}^e) and the estimated Φ parameters.

Table S2: Values of volumetric and extensive initial conversion rates, diffusivities of GVL and PeOH and estimated Φ parameters.

Reactant	r_i^{0V} (mol s^{-1} cm^{-3})	r_i^0 (mol s^{-1})	D_{ij} (cm^2 s^{-1})	D_{ij}^e (cm^2 s^{-1})	Φ_i
GVL	2.84 x10^{-8}	1.19 x10^{-6}	2.18 x10^{-4}	3.64 x10^{-5}	1.30 x10^{-5}
PeOH	5.98 x10^{-8}	2.51 x10^{-6}	1.83 x10^{-3}	3.05 x10^{-4}	1.39 x10^{-7}

In both cases, for GVL and PeOH, the Φ value was significantly lower than 1, indicating that the intraparticle mass transfer limitations were negligible for both reactants according to the Weisz-Pratter criterion.

At the light that neither external nor internal significant mass transfer limitations exist in the experimental conditions employed in this work, it is possible to affirm that the differences in catalytic activity among the SA samples are due to differences in the nature, strength and density of acid sites.

References

[1] K.G. Martínez Figueredo, D.J. Segobia, N.M. Bertero, Catal. Commun. 144 (2020) 106087.

[2] (n.d.).

[3] C.E. Chan-Thaw, M. Marelli, R. Psaro, N. Ravasio, F. Zaccheria, RSC Adv. 3 (2013) 1302–1306.

[4] S.A. D'Ippolito, L. Pirault-Roy, C. Especel, F. Epron, C.L. Pieck, RSC Adv. 7 (2017) 46803–46811.

[5] K.G. Martínez Figueredo, E.M. Virgilio, D.J. Segobia, N.M. Bertero, Chempluschem 86 (2021) 1342–1346.

[6] A. Corma, C. Corell, W. Kolodziejski, J. Prez-pariente, I.D.T. Quimica, U. Polit, D. Valencia, Zeolites 2449 (1995) 576–582.

[7] J.B. Peri, J. Phys. Chem. 70 (1966) 3168–3179.

[8] P.A. Ramachandran, R.V. Chaudhari, Three-Phase Catalytic Reactors, Gordon and Breach Science Publishers, 1983.

[9] P.B. Weisz, C.D. Prater, Adv. Catal. 6 (1954) 143–196.

[10] Y. Sano, N. Yamaguchi, T. Adachi, J. Chem. Eng. Japan 7 (1974) 255–261.

[11] A. Vignes, Ind. Eng. Chem. Fundam. 5 (1966) 189–199.

[12] C.R. Wilke, P. Chang, AIChE J. 1 (1955) 264–270.
[13] P.S. Badajoz, D. García-Vera, I. Montesdeoca, D.E. Santiago, A. Marrero-Pérez, P. Herrera-Vega, G. Pérez-Riverol, Afinidad. J. Chem. Eng. Theor. Appl. Chem. 79 (2022) 447–458.
[14] K.A. Reddy, L.K. Doraiswamy, Ind. Eng. Chem. Fundam. 6 (1967) 77–79.
[15] D.S. Viswanath, T. Ghosh, D.H.L. Prasad, N.V.K. Dutt, K.Y. Rani, Viscosity of Liquids. Theory, Estimation, Experiment, and Data, Springer, The Netherlands, 2007.
[16] K.G. Martínez Figueredo, D.J. Segobia, N.M. Bertero, Energy Convers. Manag. X 13 (2022) 100162.